Available at www.sciencedirect.com

ScienceDirect

journal homepage: www.elsevier.com/locate/he

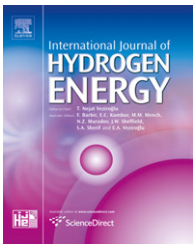

Water management studies in PEM fuel cells, part III: Dynamic breakthrough and intermittent drainage characteristics from GDLs with and without MPLs

*Zijie Lu, Michael M. Daino, Cody Rath, Satish G. Kandlikar**

Mechanical Engineering Department, Rochester Institute of Technology, 76 Lomb Memorial Dr., Rochester, NY 14623, USA

ARTICLE INFO

Article history:
Received 26 November 2009
Received in revised form
6 January 2010
Accepted 6 January 2010
Available online 16 March 2010

Keywords:
PEM fuel cell
Water management
Gas diffusion layer
Water transport
Dynamic breakthrough
Intermittent drainage

ABSTRACT

The transport of liquid water and gaseous reactants through a gas diffusion layer (GDL) is one of the most important water management issues in a proton exchange membrane fuel cell (PEMFC). In this work, the liquid water breakthrough dynamics, characterized by the capillary pressure and water saturation, across GDLs with and without a microporous layer (MPL) are studied in an ex-situ setup which closely simulates a real fuel cell configuration and operating conditions. The results reveal that recurrent breakthroughs are observed for all of the GDL samples tested, indicating the presence of an intermittent water drainage mechanism in the GDL. This is accounted for by the breakdown and redevelopment of the continuous water paths during water drainage as demonstrated by Haines jumps. For GDL samples without MPL, a dynamic change of breakthrough locations is observed, which originates from the rearrangement of the water configuration in the GDL following the drainage. For GDL samples with MPL, no dynamic change of breakthrough location can be found and the water saturation is significantly lower than the samples without MPL. These results suggest that the MPL not only limits the number of water entry locations into the GDL (such that the water saturation is drastically reduced), but also stabilizes the water paths (or morphology). The effect of MPL on the two-phase flow dynamics in gas channels is also studied with multi-channel flow experiments. The most important result is that GDL without MPL promotes film flow and shifts the slug-to-film flow transition to lower air flow rates, compared with the case of GDL with MPL. This is closely related to the larger number of water breakthrough locations through GDL without MPL, which promotes the formation of water film.

1. Introduction

Improved transport of liquid water and reactant gases through the electrodes in proton exchange membrane fuel cells (PEMFCs) has been the subject of intense studies due to its critical importance to fuel cell performance, freezing and cold start, and durability [1–3]. Among these, the liquid transport and the concurrent two-phase flow in the gas diffusion layer (GDL) is the most widely studied. Commonly used GDL materials for PEMFCs are carbon fiber based paper and cloth. These materials are highly porous (having porosities of about 80%) to allow reactant gas transport to the

Abbreviations: PEMFC, Proton exchange membrane fuel cell; GDL, Gas diffusion layer; MPL, Microporous layer; PTFE, Polytetrafluoroethylene; MEA, Membrane-electrode assembly.

* *Corresponding author*. Fax: +1 585 475 7710.
E-mail address: sgkeme@rit.edu (S.G. Kandlikar).

0360-3199/$ – see front matter © 2010 Professor T. Nejat Veziroglu. Published by Elsevier Ltd. All rights reserved.
doi:10.1016/j.ijhydene.2010.01.012

Nomenclature

Ca	capillary number
M	viscosity ratio
u	velocity (m/s)
μ	viscosity (Pa·s)
σ	surface tension (N/m)
P_c	capillary pressure (Pa)
S_w	water saturation
P	pressure (Pa)
P_b	breakthrough pressure (Pa)
V_p	GDL pore volume (m^3)
m_W	mass of water in GDL (kg)
ρ	density (kg/m^3)
A	cross-sectional area (m^2)
δ	GDL thickness (m)
ε	GDL porosity
R_c	equivalent capillary radius (m)
θ	contact angle (degree)

Subscript

nw	non-wetting
W	water
air	air

catalyst layer, as well as liquid water transport from the catalyst layer. In order to facilitate the removal of liquid water, GDLs are typically coated with a non-wetting polymer such as polytetrafluoroethylene (PTFE) to make them hydrophobic. Additionally, a fine microporous layer (MPL), consisting mainly of carbon powder and PTFE particles, is generally applied to the GDL side facing the MEA (membrane-electrode assembly) to further increase cell performance. The extreme structural and chemical heterogeneity of GDLs substantially complicates the studies of liquid water transport and associated mass transport losses [4,5].

The transport of liquid water through a GDL is a drainage process in which water, as a non-wetting fluid, displaces the wetting fluid, air. When water is injected at a low constant rate (thus negligible viscous forces), the displacement will be dominated by capillary forces. Notably at normal fuel cell operating conditions, the capillary number ($Ca=(u\mu_{nw})/\sigma$, in the range of 10^{-8}–10^{-5}, where u, μ_{nw} and σ are the velocity, viscosity and surface tension respectively of non-wetting fluid) and viscosity ratio ($M=\mu_{water}/\mu_{air}$, 17.5) produce capillary-driven water flow [6,7]. One of the critical constitutive relationships for describing capillary flow in a porous material is capillary pressure versus liquid water saturation (P_c vs. S_w). This has been the focus of several recent investigations [8–10]. A permanent capillary pressure hysteresis between liquid water injection and withdrawal is generally observed. Gostick et al. [9] accounted for the capillary hysteresis in terms of the contact angle hysteresis and the pore geometric effects. It should be noted that all these works measured the GDL saturation up to 1, which may be correlated to the GDL under the ribs where the drainage of water is restricted and water remains confined in the GDL. However, for the GDL under the channels, water drainage is quite different because water in this area can be easily removed in the form of droplets and films as well as slugs, leading to a lower saturation in the GDL. Because of this fact, the GDL saturation in an operating fuel cell is non-uniformly distributed [11,12].

The dynamics of the liquid water transport through a GDL is also of interest to understand the resistance of reactant gas transport due to water accumulation. However, this has been barely studied until recently due to the difficulties of observing water transport phenomena inside the GDLs. Nam et al. [13] and Nam and Kaviany [14] observed vapor condensation and liquid breakthrough in a GDL using an environmental scanning electron microscope, and proposed a tree-like transport mechanism in which micro-droplets condensed from vapor agglomerate to form macro-droplets which eventually flow preferentially toward larger pores and breakthrough. However, this method is not possible to simulate fuel cell operating conditions due to the vacuum requirements. Pasaogullari and Wang [15] also hypothesized a tree-like water transport behavior in GDLs in their two-phase flow model. Litster et al. [16] visualized liquid water flow as it emerged from the surface and a few micrometers below the surface of a GDL using a fluorescence microscope. They observed that water emerges from preferential pathways and suggested a ''fingering and channeling'' mechanism for water transport in GDL pores. Bazylak et al. [17] found that the preferential water pathways coincided with the compression areas in the GDL, which they accounted for by a loss of GDL hydrophobicity due to the fiber breakup and PTFE coating deterioration caused by compression. In a later study, Bazylak et al. [18] observed the dynamic changes in breakthrough locations for water transport through a GDL and explained it using a dynamic and interconnected network of water pathways within the GDL. Gao et al.'s [19] confocal microscope visualization revealed an unstable ''column flow'' in GDLs, which is similar to Litster et al.'s fingering model [16], except that wider flow paths spanning several pores are observed. Manke et al. [20,21] and Hartnig et al. [22] investigated the in-situ liquid water evolution and transport in an operating fuel cell with synchrotron X-ray radiography. They observed an ''eruptive transport'' mechanism in GDL pores near the channels, which they describe as the quick ejection of droplets from the GDL into the gas channels. However, water fills continuously in the GDL pores under the central land following a capillary tree-like process [14,15]. Both the ex-situ and in-situ experiments have clearly demonstrated that there exist low resistance ''water transport channels'' within a GDL and that water transport and breakthrough are dynamic processes. However, the morphology of transport channels and the dynamics of water transport in these channels need further investigation.

Theoretical treatment of water transport in a GDL has been the focus of several models. A large number of works are based on the continuum two-phase flow model [14,15,23–25], which describes the flow and transport on the basis of Darcy's law. Unfortunately, GDL-specific experimental data on many of the necessary relationships and parameters, such as the water saturation dependent relative permeability, effective

diffusivity, and air–water capillary pressure, are scarce, making the application of these models to GDL materials questionable. As an alternative approach, a pore-network model, which has a long history in the study of porous media like soils and rocks [26], has recently been used in modeling water transport in GDL materials [27–30]. The pore-network model maps a complex pore space continuum onto a regular and irregular network of pore bodies and pore throats. Several works have shown that invasion-percolation process, which is a strongly capillary-driven process at the limiting case of zero fluid velocity, may be an important mechanism for water transport in GDL. However, most of the pore-network models [28,30] focus on the numerical determination of the macroscopic two-phase properties, such as the capillary pressure versus saturation correlation (P_c–S_w curve) and the relative phase permeability as a function of S_w, and little work has been done to clearly understand the mechanism of water transport through a GDL.

The presence of a MPL on GDLs has been shown to improve the fuel cell performance, but the roles of (or mechanisms within) MPL are not clearly understood. It has been postulated that MPL improves the fuel cell water management and mass transport, e.g., avoiding fast dry-out of the PEM at low current densities and electrode flooding at high current densities. Several authors [31,32] have demonstrated that the MPL improves the humidification of the membrane at the anode side. Jordan et al. [32] and Kong et al. [33] concluded that the MPL enhances oxygen diffusion by reducing flooding in the cathode. The critical role of MPL in reducing flooding, as a result of the modification of the pore structure (e.g., porosity, pore size distribution, hydrophobicity, and nonuniformity) of GDL, has received wider acceptance in many recent studies [34–37]. Weber and Newmann [38] and Lin and Nguyen [39] explained the function of MPL in reducing the cathode flooding as a capillary barrier, which prevents water from entering the cathode GDL and forces water to permeate from cathode to anode. However, recent experimental studies show that MPL does not significantly influence the water back-diffusion rate [40,41]. Alternatively, the role of MPL in control of water distribution has been proposed in the theoretical treatment of water saturation distribution in multi-layer electrodes [13,14]. The authors suggest that the MPL reduces the water saturation in GDL near the catalyst layer and therefore improves the cell performance. In this way, the MPL enhances the cathode water transport rather than hindering it. Gostick et al. [42] measured the water saturation and associated capillary pressure at the point of water breakthrough in GDL samples with and without MPL. Their data demonstrated that the GDL saturation at water breakthrough is drastically reduced in the presence of MPL, suggesting that an MPL restricts the number of points of entry of water into the GDL. However, pore scale phenomena associated with the movement of liquid water and its interplay with GDL pore structure and wettability warrant further investigation.

This work is designed to investigate the water transport dynamics through GDLs and its effect on the two-phase flow in fuel cell gas channels. For this purpose, ex-situ setups, which have been designed to study the two-phase flow dynamics in fuel cell gas channels under typical fuel cell operating conditions [43,44], are modified and used. Two types of GDLs, SGL and Grafil, with and without MPL, are studied and compared. Capillary pressure as a function of time before and after breakthrough is recorded and the water saturation is determined for each sample. A transport mechanism is proposed on the basis of the experimental data. The effects of MPL on the water transport in GDL and the consequent two-phase flow in gas channels are discussed.

2. Experimental

2.1. Materials

Two types of GDLs, SGL 25 (SGL Carbon Group, Wiesbaden, Germany) and Grafil U-105 (Mitsubishi Rayon Corp., Otake City, Japan), with and without MPL coating, were studied in this work (Table 1). SGL GDLs were purchased from Ion Power (Delaware) and Grafil U-105 GDLs were provided by General Motors. All of these GDLs are carbon paper based and treated with PTFE to increase their hydrophobicity. SGL 25BC sample had a 30–50 μm thick MPL on one side and Grafil U-105B had a10 μm thick MPL. Fig. 1 shows images of the two GDLs. These two types of GDLs were chosen because they had similar GDL pore structure, thickness, and in-situ fuel cell performance [45].

2.2. Water breakthrough experiment

In this experiment, liquid water was injected through the bottom surface of the GDL (the MPL side for the case of GDL with MPL) using a syringe pump (Harvard Apparatus 11 Plus) connected to a water chamber in a Polycarbonate (Lexan®) base (Fig. 2). Eight channels, each 30 mm long, 0.7 mm wide, and 0.4 mm deep with a land width of 0.5 mm between adjacent channels, were formed on the top surface of the Lexan base to distribute water uniformly over the GDL surface. The channel shape is of weaving type with an 11° angular channel switchback every 5 cm. These water channels were connected to the water chamber through an array of 3 holes for each channel. The channel dimensions correspond to a total GDL pore volume of 27–30 μL, depending on the porosity of the samples, as listed in Table 1. The geometry and dimensions of these channels were derived from a real fuel cell design [44,46]. A 50 μm thick polyurethane (PU) film was used to cover the GDL bottom surface at the periphery of the water channels in order to prevent water leakage.

In order to visualize the water breakthrough locations, a layer of 0.7 mm thick Porex X-4588 wicking medium (Porex Technologies Corp., Fairburn, GA) was placed on top of the GDL. This medium is a hydrophilic high-density polyethylene (HDPE) material manufactured with uniformly distributed pores of size 80–120 μm. The Porex X-4588 material is permeable to water, thus allowing for the uptake of the emerging water and preventing it from expanding along and re-entering into the GDL. This hydrophilic medium has negligible effect on the determination of the GDL breakthrough pressure because of its negative capillary pressure. The cell was then held between two Lexan plates, which were tightened with bolts. The transparent top Lexan plate allowed the visualization of the breakthrough locations. A Nikon CCD

Table 1 – GDL Properties, water breakthrough pressures (P_b), water saturation at breakthrough ($S_{w,b}$), equivalent capillary radius corresponding to breakthrough (R_c), and information about the emergence of new break sites in different GDLs.

GDL	Structure	Thickness[a] (μm)	PTFE[b] (wt%)	Porosity (%)	V_{pore} (μL)	P_b (kPa)	$S_{w,b}$ (%)	New break locations	R_c (μm)
Grafil U-105A	No MPL	200 ± 3	7.0	87	29	7.4 ± 1.1	4.7–12.2	yes	19.5
Grafil U-105B	w/MPL	208 ± 3	7.0	80	28	12.7 ± 1.4	2.4 ± 0.2	no	11.3
SGL 25BA	No MPL	183 ± 3	5.0	88	27	1.7 ± 0.5	2.6–7.1	yes	80.9
SGL 25BC	w/MPL	225 ± 3	5.0	80	30	6.7 ± 1.2	0.8 ± 0.2	no	21.5

a Thickness was measured with a micrometer.
b PTFE content was taken as the manufacturer value.

camera (Coolpix P80, Tokyo, Japan) was used to collect the images during the experiments.

Liquid water was delivered at a rate of 10 μL/min, unless otherwise stated. This inlet water injection rate corresponded to equivalent water production rate at current density of about 1.2 A/cm^2 (without consideration of the condensation from the humidified gas streams and the water transport between anode and cathode in a real operating fuel cell) and a capillary number in the order of 10^{-6}. The liquid pressure referenced to the atmospheric pressure was measured with a differential pressure transducer (Honeywell FDW2AR), which was placed close to the water chamber in the Lexan base and was recorded with a DAQ system (National Instruments, Austin, TX) at 100 Hz. The pressure transducer had an operating range of 0–15 kPa with a precision of 0.2% over the entire range. Assuming that air in the GDL is at equilibrium with the surrounding environment, the transducer directly measures the capillary pressure, which is expressed as the following in this work:

$$P_c = P_{water} - P_{air} \quad (1)$$

where P_{water} is the liquid pressure at one side of the meniscus and P_{air} is the air pressure at the other side of the meniscus within the GDL.

Preliminary experiments demonstrated that at a constant water injection rate a large pressure spike was always obtained at breakthrough. These large pressure spikes were also reported in literature [18,19]. However, such a pressure spike complicates the accurate determination of the breakthrough pressure because it may coincide with the pulses of syringe pump itself (at very low flow rates the syringe pump does not operate in a true continuous mode). Therefore, in order to better determine the capillary pressure, a step-wise water injection was used. In this step procedure, the syringe pump runs for a set time and is then shut off for a set time. This allows the water pressure to relax to a new equilibrium value. Experiment showed that the combination of a running time of 120 s and a stop time of 60 s gave the best result. Fig. 3 shows a transient response of capillary pressure to changes in water volume in a step-wise cycle of 120 s-run/60 s-stop. After the first breakthrough was observed, the step-wise procedure was stopped and the water was injected at a preset (constant) flow rate until the end of the experiment.

After the water breakthrough experiment, the GDL sample was quickly removed from the test section. The surface water was removed with a hydrophilic tissue (Kimtech) and the weight of the wet GDL sample was measured. The sample was then dried in the vacuum at room temperature for several hours and the dry sample weight was measured again. The difference of these two weights revealed the mass of water inside the GDL, from which the water saturation was computed:

$$S_W = \frac{V_W}{V_P} = \frac{m_W \cdot \rho^{-1}}{A\delta\varepsilon} \quad (2)$$

where V_W is the volume of water in the sample, V_P is the GDL pore volume, m_W is the mass of water in the sample, ρ is the density of water, A is the total cross-sectional area, δ is the GDL thickness and ε is the porosity. The thickness of each sample was measured directly with a micrometer while the porosity was taken from the manufacturer documentation. It should be noted that this method may underestimate the

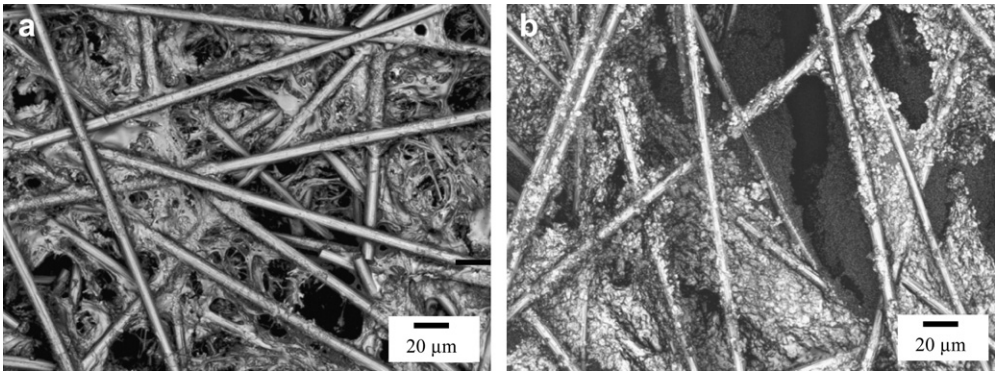

Fig. 1 – Images from a Keyence Confocal Laser Scanning Microscopy for (a) Grafil and (b) SGL GDL.

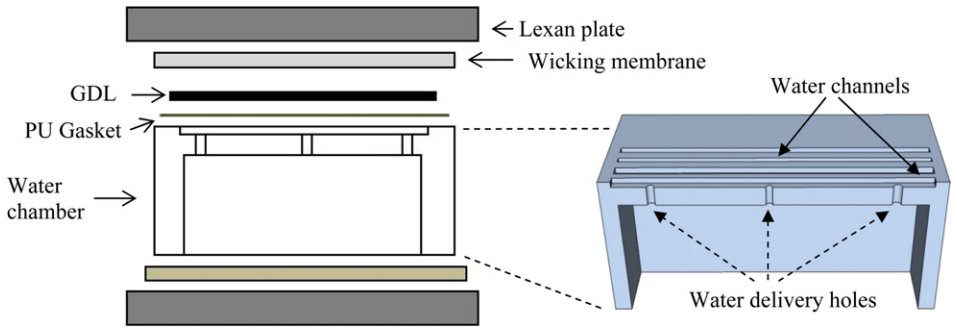

Fig. 2 – Schematic of the water breakthrough experimental setup and a 3D view of the water chamber.

water saturation because of the drying procedure. However, it was not our intention to precisely determine the water saturation. Instead, the saturation measurement was solely for comparison between different GDL samples.

2.3. *Multi-channel two-phase flow experiment*

An ex-situ multi-channel test setup was designed in the authors' lab to study the two-phase flow and water transport dynamics in PEMFC gas channels [43,44]. The test section consisted of a GDL sandwiched between an air channel plate and a water chamber plate. The air flow field consists of eight parallel channels, each having a rectangular shape of 0.7 mm wide, 0.4 mm deep and 183 mm long, and an 11° angular channel switchback every 5 cm. The geometries and dimensions, except for the channel length, were identical to the channels used in the water breakthrough experiment. The air channels are made of vapor polished Lexan which allows for visualization of the two-phase flow patterns. The water plate contained four separate water chambers, which allowed for uniform water supply to the GDL surface, with the water flow to each chamber independently controlled by a syringe pump. This setup simulated the cathode side of a PEMFC. Detailed description of the experimental setup is available in Refs. [43,44].

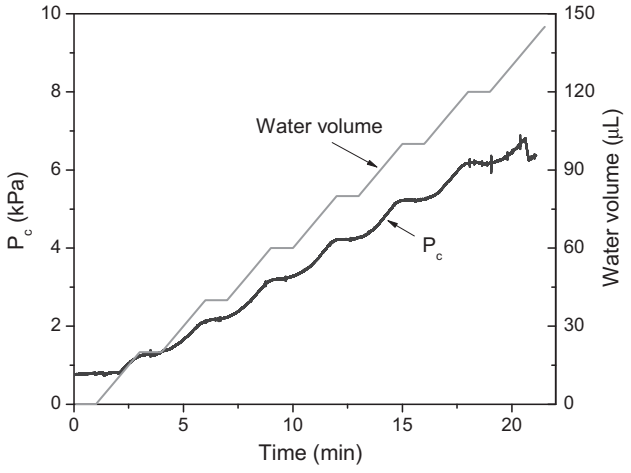

Fig. 3 – Typical response of the capillary pressure P_c as well as the injected water volume in a step-wise water intrusion experiment for SGL 25BC.

Dry air was supplied from a Zero Air Generator (Parker HPZA-30000, Haverhill, MA) and the flow rate was controlled via a bank of mass flow meters (Omega FL3861C, FL3804G, FL3805ST). De-ionized water (18.2 MΩ, Millipore) was delivered to each of the four water chambers through four syringe pumps (Harvard). The water pressure in each chamber referenced to atmospheric air pressure was measured with a pressure transducer (Omega PX26). Visualization of the two-phase flow was conducted using a Photron high speed camera.

During the course of experiments, the air and water flow rates were controlled within typical operating conditions of PEMFCs corresponding to superficial gas velocities between 0 and 30 m/s (Reynolds numbers in the range of 0–960) and the superficial liquid velocities between 0 and 0.0015 m/s. These test conditions were equivalent to fuel cell operating conditions with a current density range of 0–2 A/cm^2 and a maximum air stoichiometry of 30. All the experiments were conducted at ambient temperature and pressure conditions.

3. Results

3.1. *Water breakthrough in GDL samples without MPL*

Fig. 4 shows a typical water breakthrough behavior through an initially dry SGL 25BA sample. For clarity, the capillary pressure in the pre-breakthrough period, which is similar to Fig. 3, is not displayed in this figure. The breakthrough capillary pressure for this sample, read as the first peak pressure, is 1.78 kPa.

The most outstanding feature from Fig. 4 is the dynamic characteristics of water breakthrough in the GDL. This is displayed in two aspects: the dynamic capillary pressure and the dynamic breakthrough locations. The capillary pressure initially increases until the water breaks through, as expected. After the first breakthrough, the capillary pressure does not drop to a steady-state value; instead it fluctuates and leads to more breakthroughs. Similar phenomenon is also observed for all other GDL samples. The recurrent water breakthroughs cannot be accounted for by current pore-network models because most of these models assume that water flows along the same continuous paths (i.e. a network of lager pores) once it is formed during the first breakthrough. This continuous flow assumed by pore-network models predicts a constant pressure after breakthrough [29]. In contrast, the dynamic

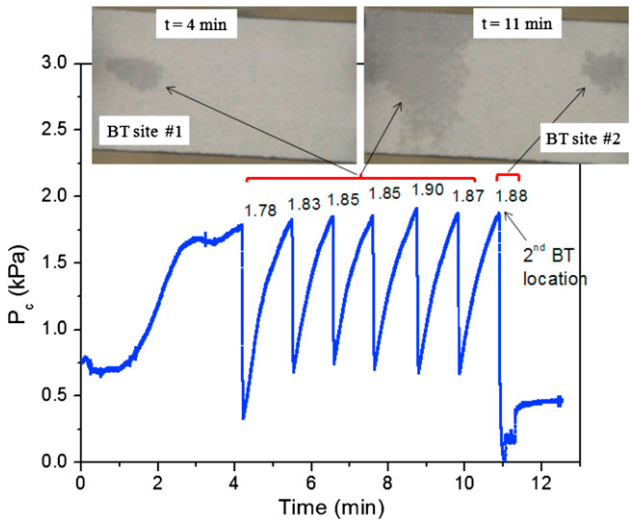

Fig. 4 – Water breakthrough behavior through an initially dry SGL 25BA sample. The inserted images are still pictures taken from videos. The numbers in the figure indicate the peak pressures. BT denotes "breakthrough".

capillary pressure observed in Fig. 4 reveals a breakdown of the water paths caused by the water drainage on the GDL surface. This will be further discussed in Section 4.

Another distinct characteristic is the dynamic water breakthrough locations, i.e., the breakthrough location changes with time, as illustrated by the inserted images in Fig. 4. As shown in Fig. 4, water was found to emerge from just a few preferential locations on the GDL surface. After the first breakthrough at an initial location, five more distinct breakthrough events occur at the same location until a new breakthrough site is observed 7 min after the initial breakthrough. The change of breakthrough location was not a random phenomenon, but commonly observed in other SGL 25BA samples, as summarized in Table 2. Bazylak et al. [18] observed a similar phenomenon with fluorescence microscopy and they accounted for the phenomenon in terms of the branching of the network of water pathways. However, we found this phenomenon was closely related to the dynamic capillary pressure. A detailed analysis based on this observation is given in Section 4. It should be noted that this dynamic water breakthrough location phenomenon is also unaccounted for by current pore-network models.

Table 2 – Water breakthrough scenario in SGL 25BA samples.

Sample No	Breakthrough situation
1	Second breakthrough site after 3 consecutive bursts in the first site
2	Second breakthrough site after 6 consecutive bursts in the first site
3	Two new breakthrough sites after 4 consecutive bursts in the first site
4	Second breakthrough site after 4 consecutive bursts in the first site
5	Only one breakthrough site observed on the edge of water channel
6	Second breakthrough site after 5 consecutive bursts in the first site

The GDL water saturation after the breakthrough experiment was measured and the results are shown in Table 1. Due to the dynamic water breakthrough behavior, a wide range of saturation, from 2.6 % to 7.1%, was obtained from sample to sample.

The water breakthrough behavior through the Grafil U-105A sample (without MPL) was largely similar to that of SGL 25BA. Fig. 5 shows an example of such experiments. Multiple breakthrough events and dynamic breakthrough locations were also clearly observed. However, important differences between the breakthroughs of the two samples can still be found. The Grafil U-105A sample displayed a significantly higher breakthrough pressure (7.4 kPa vs. 1.8 kPa) and greater water saturation than the SGL 25BA sample, as shown in Table 1.

It is generally accepted that the capillary pressure in porous media describes the throat diameters in a void (or pore) network. The critical capillary size corresponding to the breakthrough can be calculated from the breakthrough pressure based on the Young–Laplace equation:

$$P_c = \frac{2\sigma\cos\theta}{R_c} \quad (3)$$

where R_c is the equivalent capillary radius, σ (=0.072 N/m) surface tension for water, θ contact angle of water inside GDL pores, approximately taken as the contact angle of water on

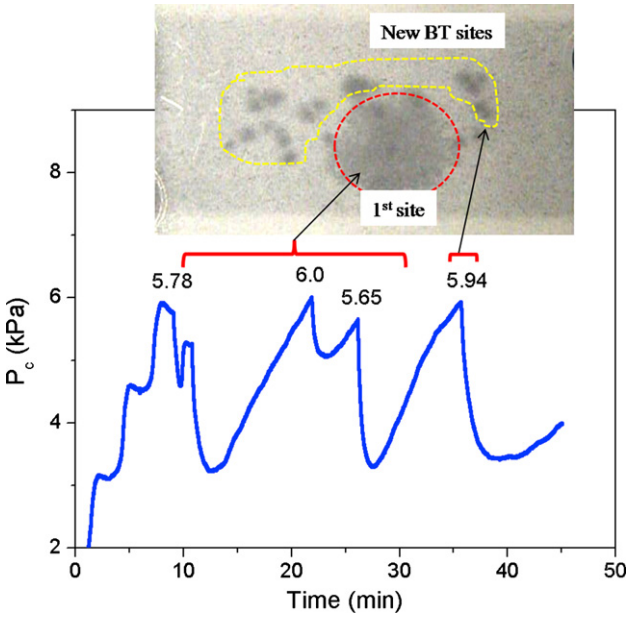

Fig. 5 – Water breakthrough behavior through an initially dry Grafil U-105A sample. The inserted still picture, taken from the corresponding video, displays the new breakthrough sites. Note that the contrast has been increased in the inset image to highlight water breakthrough locations. The numbers in the figure indicate the peak pressures. BT denotes "breakthrough".

PTFE sheet (120°). Through Eq. (3), the critical capillary diameter for Grafil U-105A was calculated to be 19.5 μm (see Table 1), which is close to the mean pore size of the GDL, while SGL 25BA showed a critical capillary diameter of about 81 μm. This difference in the critical size is related to both the fibrous structure and the internal wettability. As shown in Fig. 1, Grafil U-105A displays pores (or voids) of slightly smaller size than SGL 25BA. Furthermore, Grafil U-105A shows many fine web structures, which may further decreases the pore size. The higher PTFE content of 7 wt% in Grafil U-105A will also increase the breakthrough pressure and thus decrease the critical throat size compared to the 5 wt% PTFE in SGL 25BA. Nonetheless, the critical throat size of 81 μm in SGL 25BA is significantly larger than its mean pore size, which may indicate that the internal contact angle is much smaller than 120°.

3.2. *Water breakthrough in GDL samples with MPL*

GDLs used in fuel cell applications are normally coated with a microporous layer (MPL) to improve the cell performance at high current densities. Due to water flooding and severe mass transport losses that usually occur in this regime, MPL is sometimes referred to as the water management layer. In this work, the water breakthrough in GDLs with MPL was also investigated. In these tests, the MPL was placed facing the water inlet. The case in which the MPL was away from the water inlet was not tested, due to the fact that this configuration is rarely used in fuel cell operation.

In general, the Grafil U-105B, which has a very thin (about 8 μm) MPL layer, and SGL 25BC, which has a MPL of about 40 μm thickness, exhibited similar water breakthrough behaviors. Fig. 6 shows the water breakthrough behavior through an initially dry SGL 25BC sample, as a typical example. Multiple breakthroughs are observed, similar to the cases of GDLs without MPL, indicating that the breakthrough process is dynamic. However, no shifting of water breakthrough locations was observed in either Grafil U-105B or SGL 25BC samples, which suggests that water flows in the same preferential paths inside the GDL and emerges at the same location on the GDL surface formed in the initial breakthrough. This is in sharp contrast to the GDL samples without MPL (see Figs. 4 and 5) in which the changing of breakthrough locations is always observed. This difference must originate from the MPL, suggesting that the MPL plays a role in stabilizing the preferential water pathways.

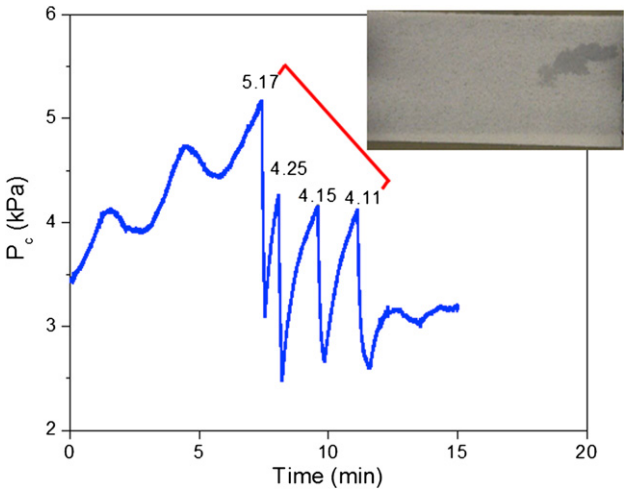

Fig. 6 – Water breakthrough behavior through SGL 25BC sample. The inserted image is the still picture taken from the video and reveals the water breakthrough location.

The breakthrough capillary pressure and the water saturation in these samples were also determined and are shown in Table 1. Generally, the GDLs with a MPL have higher breakthrough pressures compared to the corresponding GDLs without a MPL. This is expected because of the additional water flow resistance caused by the MPL, which has much smaller pore sizes and therefore a higher capillary pressure. Considering a mean pore size of 0.5 μm, which is normal for a microporous layer, the MPL could yield a breakthrough capillary pressure of about 300 kPa for this layer, according to Eq. (3). However, the breakthrough pressures for both Grafil U-105B and SGL 25BC are in the same magnitude to the corresponding samples without MPL, e.g. 12.7 kPa vs. 7.4 kPa for Grafil samples and 6.7 kPa vs. 1.7 kPa for SGL samples. This indicates that the MPLs on these samples do not function as a distinct uniform layer, because, otherwise, these layers would produce a much higher capillary pressure given their smaller pore size (and possibly higher hydrophobicity). Instead, water flows through the defects in the MPLs. Fig. 7 shows the MPL on both GDLs. From this figure, the MPL on Grafil U-105B is relatively uniform, but is very thin (around 8 μm) and barely covers the graphite fibers. These discontinuous parts of MPL along the fibers offer preferential paths for water to penetrate and therefore a much smaller breakthrough pressure, e.g. 12.7 kPa instead of 300 kPa, is obtained. Likewise, although the MPL on SGL 25BC is thicker (about 40 μm), it contains many large cracks with dimension on the order of tens of micrometers (see Fig. 7). These cracks again provide the preferential water transport pathways through the MPL and decrease the breakthrough pressure radically. These findings may be specific to the GDL materials studied here, but it is interesting to note that the defects in the MPL may be beneficial to fuel cell water management. Furthermore, additional gains could be made in fuel cell water management provided the defects in MPL were precisely controlled.

Much lower water saturations are observed for GDLs with MPL than GDLs without MPL. For example, the saturation S_w for Grafil U-105B and SGL 25BC were 2.4% and 0.8%, respectively. The measured saturation for SGL 25BC was close to the reported value of 3% for SGL 10BB obtained by Gostick et al. [42]. These saturation values were three to eight times lower than those of the corresponding samples without MPL. This result indicates that MPL can greatly reduce the water saturation in GDL. A similar result has been reported in literature and was explained by the limitation of water access to the GDL by the MPL [13,42].

3.3. *Multichannel two-phase flow experiment*

In our previous work, we have studied the two-phase flow in gas channels with ex-situ multi-channel experiment [43]. Different flow patterns, namely slug flow (defined as water

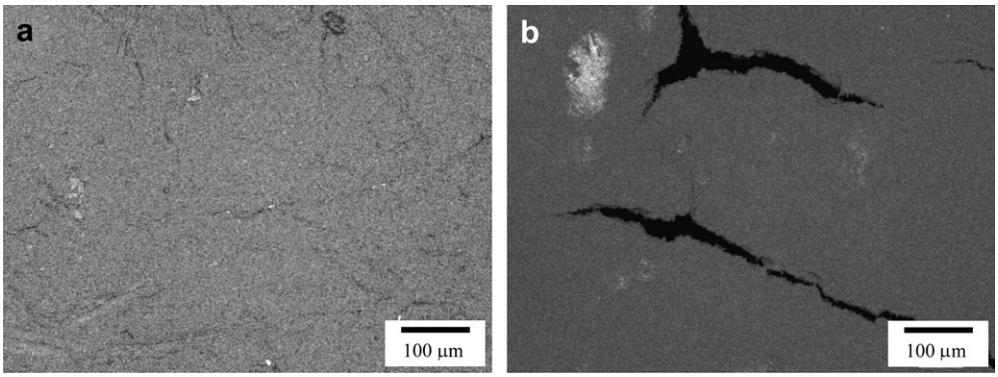

Fig. 7 – Images of microporous layer (MPL) from a Keyence Confocal Laser Scanning Microscopy on (a) Grafil U-105B and (b) SGL 25BC.

columns bridging two side walls of flow channels and displaying meniscus), film flow (defined as water buildup on one side of flow channels, either in the shape of elongated droplets or water films) and mist flow (a flow pattern in which no obvious liquid water is observed in the entire flow channels), were observed at different flow conditions. The flow pattern map was shown to provide a tool to characterize the two-phase flow dynamics in gas channels. In this work, the same method was used to study the effect of GDL samples on the channel flow dynamics.

Figs. 8 and 9 show the comparisons of the flow pattern maps in gas channels for Grafil and SGL GDLs, with and without MPL. In these figures, the superficial water velocity is plotted against the logarithmic superficial air velocity. A significant effect of MPL on channel two-phase flow dynamics was observed. The most outstanding result was that the GDL without MPL increased the tendency of film flow. For example, it shifted the slug-to-film flow transition to a greatly lower superficial air velocity and completely eliminated the mist flow pattern in the high air flow regime compared to the case of GDL with MPL. The visualization of the gas channel and the GDL surface revealed that a lot more water emergence sites were observed in the GDL without MPL compared to the sample with MPL, as demonstrated in Fig. 10 for the case of Grafil GDLs. Some of the breakthrough locations are highlighted with arrows in Fig. 10. Similar observations were also made for SGL GDLs. A direct consequence of this difference is that water transports out of the GDL sample without MPL more uniformly across the entire surface, favoring the formation of water film along the channel wall. In contrast, water emerges from GDLs containing an MPL through just a few locations, which leads to the formation of long slugs. This is closely related to their respective water transport mechanisms in these GDLs. The GDL without MPL features dynamic breakthrough locations, leading to a larger number of breakthrough locations, while the GDL with MPL has only limited breakthrough locations.

4. Discussion

The water breakthrough in GDLs has been found to occur at a few preferential locations in both Grafil and SGL types of GDLs, with the dynamic characteristics of this process having been observed. The dynamic behavior was reflected in two aspects: dynamic capillary pressure (or recurrent breakthroughs) and dynamic breakthrough locations (or changing of breakthrough locations with time). The former is commonly observed in all GDLs, while the latter is observed only in GDLs without MPL. Generally, very small water saturations, less than

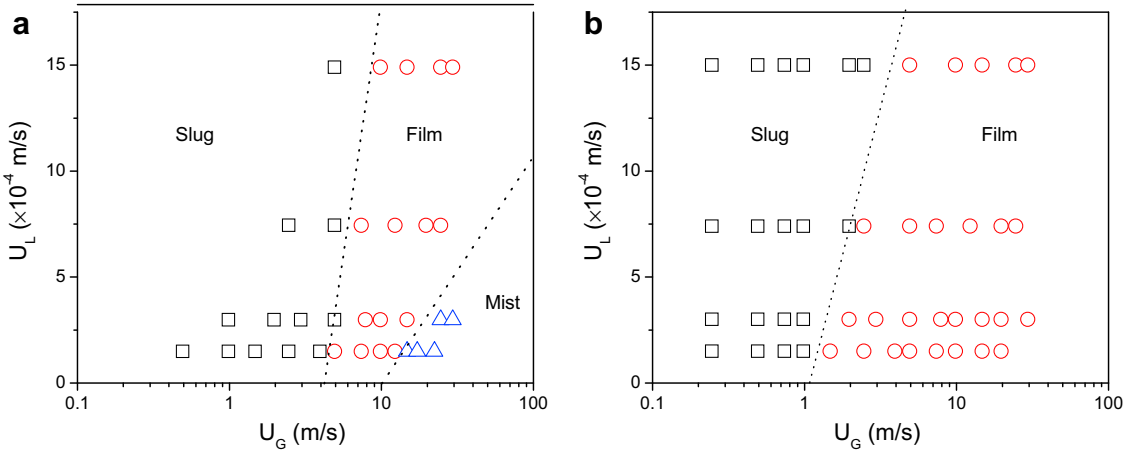

Fig. 8 – Flow pattern maps for (a) Grafil U-105B (with MPL) and (b) Grafil U-105A (without MPL).

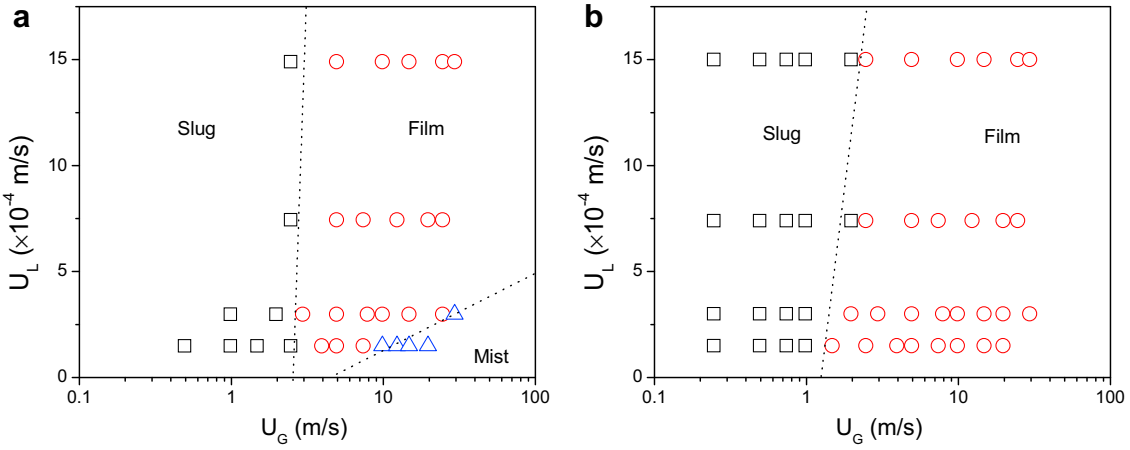

Fig. 9 – Flow pattern maps for (a) SGL 25BC (with MPL) and (b) SGL 25BA (without MPL).

10%, were observed for both GDLs at breakthrough. The low water saturations, combined with the observation of preferential breakthrough locations, may reveal an anisotropic, heterogeneous flow process in GDL. Moreover, if water flows in isotropic, homogeneous pattern, a much higher water saturation and significantly larger number of breakthrough locations would result. The anisotropic, heterogeneous water flow inside a GDL forms fast ''water transport channels'', which are more or less straight or column-like. These channels are essentially similar to the ''fingering and channeling'' observed by Litster et al. [16], the ''column flow'' observed by Gao et al. [19], and the ''eruptive mechanism'' observed by Manke et al. [20,21].

A possible interpretation of the observed phenomena can be explained in terms of Haines jumps, a description of the discontinuous drainage displacement employed in geological disciplines [26,46]. In slow drainage, when a non-wetting fluid slowly displaces a wetting fluid in porous media (e.g., water displaces air in GDL), the displacement is controlled solely by the pressure difference between the two fluids. Restrictions in the pore-throat structure of the porous medium hinder the fluid from advancing linearly. The interfaces between fluids may remain unmoved even when the pressure in the displacing fluid increases. Once the invading fluid pressure exceeds the capillary pressure at the largest restriction, the invading fluid will suddenly move into the adjacent pores, and quite often through one or more of these restrictions simultaneously. This process is usually accompanied by a negative capillary pressure drop as a result of the readjustment of the interfaces between fluids and porous medium. This localized bursting of the advancing non-wetting fluid into the initially saturated porous medium is a step-wise process of drainage, and has been called avalanches, Haines jumps, or bursts in the literature [26,46].

The transition (bursting) of water from GDL into the gas channels is triggered by the same factors as within the GDL by considering the gas channels as a new porous medium which has much larger pore size than GDL. At the breakthrough point, the bursting droplet (formed on the GDL surface) carries away water from adjacent GDL pores as it grows spontaneously. However, the supply of water is often not sufficient for the droplet to fill the larger pore (i.e. gas channel). This ''choke-off''

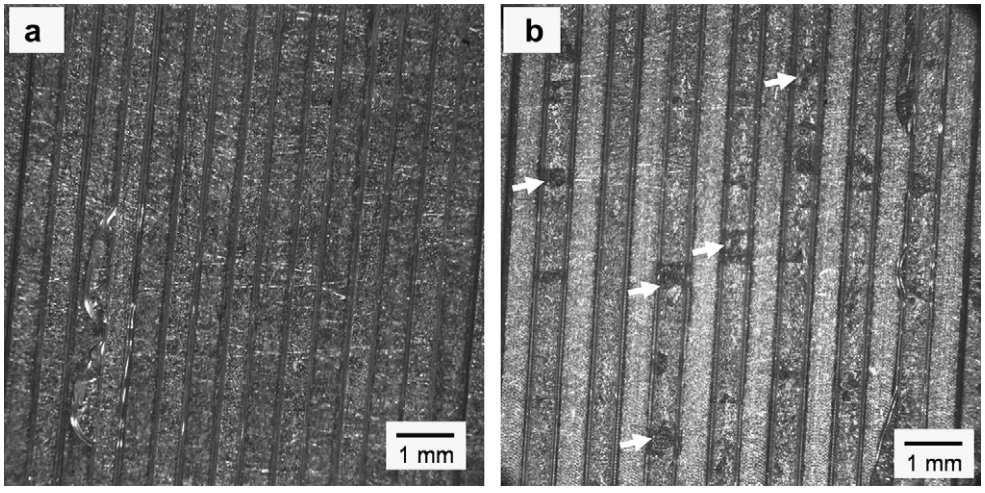

Fig. 10 – Comparison of water flow structure in gas channels combined with (a) Grafil U-105B and (b) Grafil U-105A at UG = 7.4 m/s and superficial water velocity of UL = 7.4 × 10−4 m/s. Several water emergence locations in the channels are indicated by the arrows.

effect leads to empty pores in the GDL, which breakdown the continuous water paths. These emptied pores are refilled afterwards as water is constantly injected and the bursting process occurs again, leading to the recurrent breakthrough behavior. As the "choke offs" breakdown the original water paths and water spontaneously readjusts its interfaces inside GDL pores. This water/air interface relaxation process may lead to a new preferential pathway in the GDL and result in a new breakthrough location. Fig. 11 shows a schematic of such a process. Thus, through the proposed mechanism we can explain both dynamic capillary pressure behavior and the dynamic breakthrough locations.

Two effects of MPL on the water breakthrough behavior have been observed. The first one is that MPL limits the water access to GDL. The role of MPL in the control of breakthrough locations has also been observed in previous studies [13,42]. Our measurements further indicate that MPL reduces the water entries to GDLs mainly via the defects, such as cracks and breakdowns of MPL by GDL fibers. Another role of MPL in water breakthrough has been identified in this work, that is, it can stabilize the water paths/morphology in GDLs. These effects can also be accounted for by the transport mechanism proposed above. As shown in Fig. 12, the water paths in GDL without MPL are interconnected to each other and, thus, the changing of the breakthrough location by the spontaneous redistribution of water configuration after the breakthrough (bursting) is possible. However, in the case of GDL with MPL, the water paths in GDL are not interconnected due to the blocking effect of MPL. Therefore, it is less likely that the localized bursting occurring at the end of one water path will affect the configuration of other water paths, thus increasing the stability of the water paths. This effect together with the limited number of water access to GDL results in a greatly reduced number of breakthrough locations for the GDL with MPL compared to GDL without MPL. As a natural consequence, MPLs lower the GDL water saturation greatly because the saturation is proportional to the total water paths in a GDL.

Generally, only a few breakthrough locations were observed on the GDLs in the ex-situ experiment and MPL further reduces the number of breakthrough locations. However, in-situ observations in an operating fuel cell reveal a greater number of droplets (or breakthrough locations) on the GDL surface [47,48]. This disagreement may indicate the contribution of other water transport mechanisms. The transport of water vapor through MPL and GDL is one of such mechanism, especially when fuel cells operate at higher temperatures. Due to the temperature gradient across the GDL, water vapor transported from catalyst layers and MPL condenses and forms micro water droplets inside the GDL. These micro-droplets then agglomerate to form macro-droplets, which eventually flow preferentially toward larger pores and breakthrough. This water transport mechanism was first proposed by Nam and Kaviney [14] in term of "inverted tree-like water transport". A feature of this

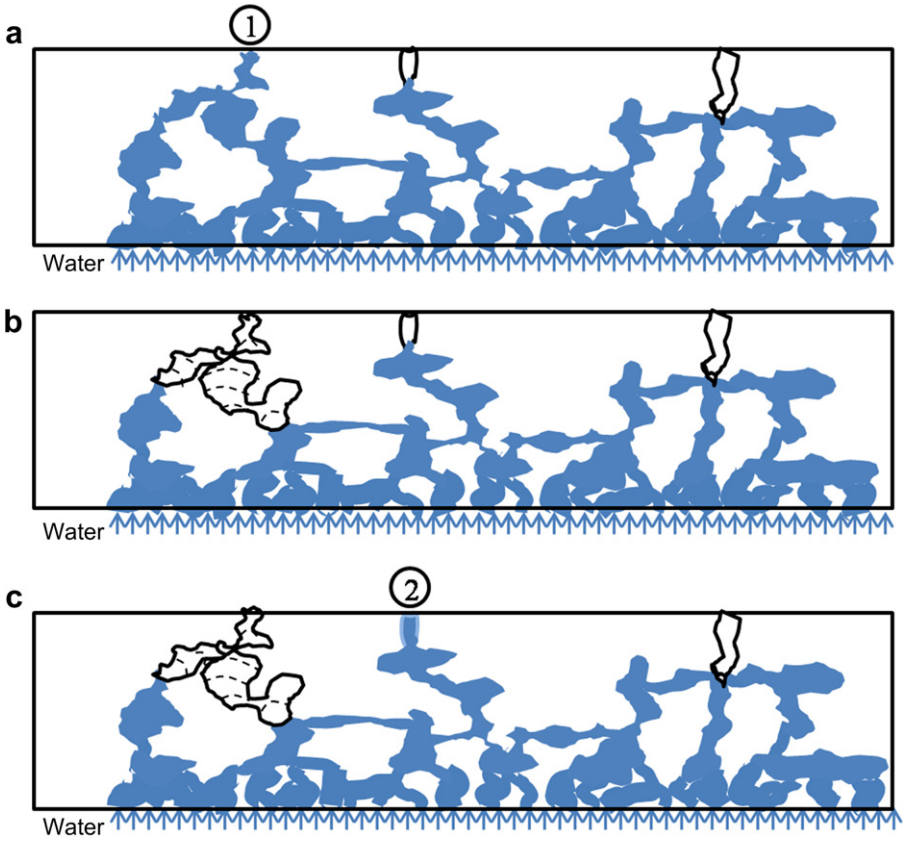

Fig. 11 – A schematic of water drainage process of a model capillary system as water emerges from GDL surface. a) 1st water breakthrough at a preferential location; b) the "choke-off" leaves empty pores in GDL and breaks down the water paths; c) spontaneous redistribution of water occurs inside GDL, which may make breakthrough at 2nd location possible.

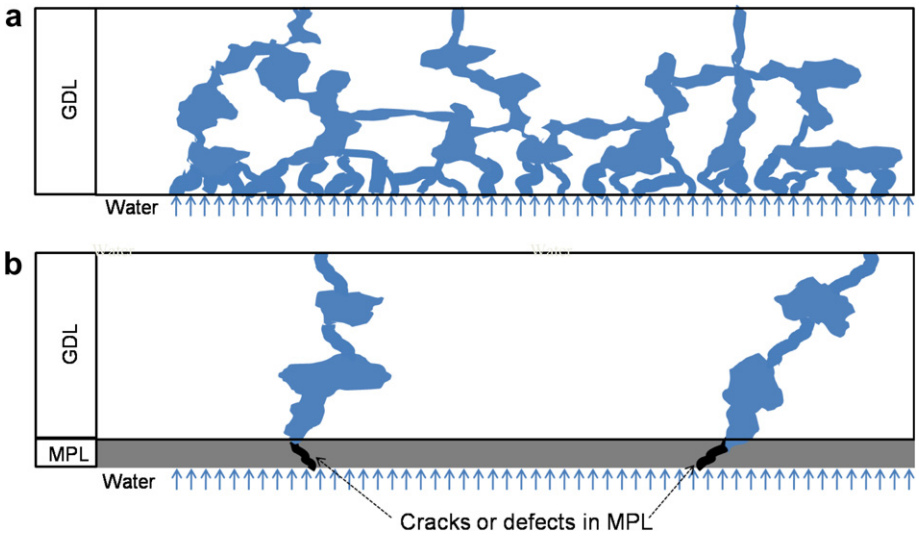

Fig. 12 – Schematic of water drainage in GDL (a) without MPL, displaying a large number of water entry points into the GDL; and (b) with MPL, restricting water entry into GDL only at the crack/defect locations in the MPL.

transport mechanism is the large number of breakthrough locations because of the large number of condensation sites in a GDL. At high fuel cell operating temperatures or high temperature gradient across GDL, the vapor condensation in the GDL is greatly increased and the contribution of the tree-like transport may eventually be dominant, producing many more breakthrough locations. This indicates that the liquid water transport through a GDL is very complicated and no single mechanism can fully describe it.

5. Conclusion

In this work, the liquid water breakthrough dynamics across GDLs with and without MPL are studied in an ex-situ setup which closely simulates a real fuel cell configuration and operating conditions. The following several points can be concluded from the results:

- The capillary pressure inside the GDL is dynamic even after the breakthrough and recurrent water breakthroughs are always observed. This indicates a breakdown and re-build of water paths caused by an intermittent water drainage process from the GDL surface.
- For GDL samples without MPL, a dynamic changing of breakthrough locations is observed, while for GDL samples with MPL no such phenomenon can be found. At the same time, the water saturation for GDLs with MPL is significantly lower than the samples without MPL. These results suggest that the MPL not only limits the number of the water entries into the GDL (so that the water saturation is drastically reduced), but also stabilizes the water paths (or morphology).
- A water transport mechanism, guided by Haines jumps, is proposed to account for the dynamic breakthrough behaviors through a GDL.
- The effect of MPL on the two-phase flow dynamics in gas channels is also studied with multi-channel flow experiments. The most important result is that GDL without MPL promotes film flow and shifts the slug-to-film flow transition to the lower air flow rates, compared with the case of GDL with MPL.

Acknowledgements

The authors gratefully thank Dr. Thomas Trabold and Mr. Jon Owejan at the General Motors Fuel Cell Research Laboratory at Honeoye Falls, New York for their technical collaboration. This work was supported by the US Department of Energy under contract No. DE-FG36-07G017018.

REFERENCES

[1] Wang CY. Fundamental models for fuel cell engineering. Chem Rev 2004;104:4727–66.
[2] Kandlikar SG. Microscale and macroscale aspects of water management challenges in PEM fuel cells. Heat Tran Eng 2008;29:575–87.
[3] Berg P, Promislow K, St. Pierre J, Stumper J, Wetton B. Water management in PEM fuel cells. J Electrochem Soc 2004;151: A341–53.
[4] Gostick JT, Fowler MW, Ioannidis MA, Pritzker MD, Volfkovich YM, Sakars A. Capillary pressure and hydrophilic porosity in gas diffusion layers for polymer electrolyte fuel cells. J Power Sources 2006;156:375–87.
[5] Quick C, Ritzinger D, Lehnert W, Hartnig C. Characterization of water transport in gas diffusion media. J Power Sources 2009;190:110–20.
[6] Sinha PK, Wang CY. Pore-network modeling of liquid water transport in gas diffusion layer of a polymer electrolyte fuel cell. Electrochim Acta 2007;52:7936–45.
[7] Medici EF, Allen JS. Existence of the phase drainage diagram in proton exchange membrane fuel cell fibrous diffusion media. J Power Sources 2009;191:417–27.

[8] Fairweather JD, Cheung P, St-Pierre J, Schwartz DT. A microfluidic approach for measuring capillary pressure in PEMFC gas diffusion layers. Electrochem Commun 2007;9:2340–5.
[9] Gostick JT, Ioannidis MA, Fowler MW, Pritzker MD. Direct measurement of the capillary pressure characteristics of water–air–gas diffusion layer systems for PEM fuel cells. Electrochem Commun 2008;10:1520–3.
[10] Cheung P, Fairweather JD, Schwartz DT. Characterization of internal wetting in polymer electrolyte membrane gas diffusion layers. J Power Sources 2009;187:487–92.
[11] Turhan A, Heller K, Brenizer JS, Mench MM. Quantification of liquid water accumulation and distribution in a polymer electrolyte fuel cell using neutron imaging. J Power Sources 2006;160:1195–203.
[12] Hartnig C, Manke I, Kuhn R, Kleinau S, Goebbels J, Banhart J. High-resolution in-plane investigation of the water evolution and transport in PEM fuel cells. J Power Sources 2009;188:468–74.
[13] Nam JH, Lee KJ, Hwang GS, Kim CJ, Kaviany M. Microporous layer for water morphology control in PEMFC. Int J Heat Mass Tranf 2009;52:2779–91.
[14] Nam JH, Kaviany M. Effective diffusivity and water saturation distribution in single- and two-layer PEMFC diffusion medium. Int J Heat Mass Tran 2003;46:4595–611.
[15] Pasaogullari U, Wang CY. Liquid water transport in gas diffusion layer of polymer electrolyte fuel cells. J Electrochem Soc 2004;151:A399–406.
[16] Litster S, Sinton D, Djilali N. Ex situ visualization of liquid water transport in PEM fuel cell gas diffusion layers. J Power Sources 2006;154:95–105.
[17] Bazylak A, Sinton D, Liu ZS, Djilali N. Effect of compression on liquid water transport and microstructure of PEMFC gas diffusion layers. J Power Sources 2007;163:784–92.
[18] Bazylak A, Sinton D, Djilali N. Dynamic water transport and droplet emergence in PEMFC gas diffusion layers. J Power Sources 2008;176:240–6.
[19] Gao B, Steenhuis TS, Zevi Y, Parlange JY, Carter RN, Trabold TA. Visualization of unstable water flow in a fuel cell gas diffusion layer. J Power Sources 2009;190:493–8.
[20] Manke I, Hartnig C, Grunerbel M, Lehnert W, Kardjilov N, Haibel A, et al. Investigation of water evolution and transport in fuel cells with high resolution synchrotron X-ray radiography. Appl Phys Lett 2007;90:174105.
[21] Manke I, Hartnig C, Kardjilov N, Messerschmidt M, Hilger A, Strobl M, et al. Characterization of water exchange and two-phase flow in porous gas diffusion materials by hydrogen–deuterium contrast neutron radiography. Appl Phys Letters 2008;92:244101.
[22] Hartnig C, Menke I, Kuhn R, Kardjilov N, Banhart J, Lehnert W. Cross-sectional insight in the water evolution and transport in polymer electrolyte fuel cells. Appl Phys Letters 2008;92:134106.
[23] Weber AZ, Darling RM, Newman J. Modeling two-phase behaviour in PEFCs. J Electrochem Soc 2004;151:A1715–27.
[24] Pisani L, Murgia G, Valentini M, D'Aguanno B. A working model of polymer electrolyte fuel cells comparisons between theory and experiments. J Electrochem Soc 2002;149:898–904.
[25] Sinha PK, Wang CY. Liquid water transport in a mixed-wet gas diffusion layer of a polymer electrolyte fuel cell. Chem Eng Sci 2008;63:1081–91.
[26] Dullien FAL. Porous media: fluid transport and pore structure. New York: Academic Press; 1992.
[27] Sinha PK, Wang CY. Pore-network modeling of liquid water transport in PEM fuel cell gas diffusion layers. J Power Sources 2007;154:95–105.
[28] Gostick JT, Ioannidis MA, Fowler MW, Pritzker MD. Pore network modeling of fibrous gas diffusion layers for polymer electrolyte membrane fuel cells. J Power Sources 2007;173:277–90.
[29] Lee KJ, Nam JH, Kim CJ. Pore-network analysis of two-phase water transport in gas diffusion layers of polymer electrolyte membrane fuel cells. Electrochim Acta 2009;54:1166–76.
[30] Markicevic B, Bazylak A, Djilali N. Determination of transport parameters for multiphase flow in porous gas diffusion electrodes using a capillary network model. J Power Sources 2007;171:706–17.
[31] Qi Z, Kaufman A. Improvement of water management by a microporous sublayer for PEM fuel cells. J Power Sources 2002;109:38–46.
[32] Jordan LR, Skukla AK, Behrsing T, Avery NR, Muddle BC, Forsyth M. Effect of diffusion-layer morphology on the performance of polymer electrolyte fuel cells operating at atmospheric pressure. J Appl Electrochem 2000;30:641–6.
[33] Kong CS, Kim DY, Lee HK, Shul YG, Lee TH. Influence of pore-size distribution of diffusion layer on mass-transport problems of proton exchange membrane fuel cells. J Power Sources 2002;108:185–91.
[34] Wang XL, Zhang HM, Zhang JL, Xu HF, Tian ZQ, Chen J, et al. Micro-porous layer with composite carbon black for PEM fuel cells. Electrochim Acta 2006;51:4909–15.
[35] Wang XL, Zhang HM, Zhang JL, Xu HF, Zhu XB, Chen J, et al. A bifunctional micro-porous layer with composite carbon black for PEM fuel cells. J Power Sources 2006;162:474–9.
[36] Park GG, Sohn YJ, Yim SD, Yang TH, Yoon YG, Lee WY, et al. Adoption of nano-materials for the micro-layer in gas diffusion layers of PEMFCs. J Power Sources 2006;163:113–8.
[37] Tang HL, Wang SL, Pan M, Yuan RZ. Porosity-graded micro-porous layers for polymer electrolyte membrane fuel cells. J Power Sources 2007;166:41–6.
[38] Weber AZ, Newman J. Effects of microporous layers in polymer electrolyte fuel cells. J Electrochem Soc 2005;152:A677–88.
[39] Lin GY, Nguyen TV. A two-dimensional two-phase model of a PEM fuel cell. J Electrochem Soc 2006;153:A372–82.
[40] Karan K, Atiyeh HK, Phoenix A, Halliop E, Pharoah J, Peppley B. An experimental investigation of water transport in PEMFCs – the role of microporous layers. Electrochem Solid State Lett 2007;10:B34–8.
[41] Atiyeh HK, Karan K, Peppley B, Phoenix A, Halliop E, Pharoah J. Experimental investigation of the role of a microporous layer on the water transport and performance of a PEM fuel cell. J Power Sources 2007;170:111–21.
[42] Gostick JT, Ioannidis MA, Fowler MW, Pritzker MD. On the role of the microporous layer in PEMFC operation. Electrochem Commun 2009;11:576–9.
[43] Lu Z, Kandlikar SG, Rath C, Grimm M, Domigan W, White AD, et al. Water management studies in PEM fuel cells, part II: ex situ investigation of flow maldistribution, pressure drop and two-phase flow pattern in gas channels. Int J Hydrogen Energy 2009;34:3445–56.
[44] Kandlikar SG, Lu Z, Domigan WE, White AD, Benedict MW. Measurement of flow maldistribution in parallel channels and its application to ex-situ and in-situ experiments in PEMFC water management studies. Int J Heat Mass Tran 2009;52:1741–52.
[45] Owejan JP, Gagliardo JJ, Sergi JM, Kandlikar SG, Trabold TA. Water management studies in PEM fuel cells, part I: fuel cell design and in situ water distributions. Int J Hydrogen Energy 2009;34:3436–44.
[46] Haines WB. Studies in the physical properties of soil 5. The hysteresis effect in capillary properties and the modes of moisture distribution. J Agric Sci 1930;20:97–116.
[47] Ous T, Arcoumanis C. The formation of water droplets in an air-breathing PEMFC. Int J Hydrogen Energy 2009;34:3476–87.
[48] Yang XG, Zhang FY, Lubawy AL, Wang CY. Visualization of liquid water transport in a PEFC. Electrochem Solid State Lett 2004;7:A408–11.